Received: 25 March 2019 | Revised: 9 July 2019 | Accepted: 9 July 2019

DOI: 10.1111/jace.16692

ORIGINAL ARTICLE

Journal of the American Ceramic Society

Crystal structure and enhanced microwave dielectric properties of Ta^{5+} substituted $Li_3Mg_2NbO_6$ ceramics

Gang Wang[1] | **Dainan Zhang**[1] | **Xin Huang**[1] | **Yiheng Rao**[1] | **Yan Yang**[1] | **Gongwen Gan**[1] | **Yuanming Lai**[1] | **Fang Xu**[1] | **Jie Li**[1] | **Yulong Liao**[1] | **Cheng Liu**[1] | **Lichuan Jin**[1] | **Vincent G. Harris**[2] | **Huaiwu Zhang**[1]

[1]State Key Laboratory of Electronic Thin Films and Integrated Devices, University of Electronic Science and Technology of China, Chengdu, China

[2]Department of Electrical and Computer Engineering, Center for Microwave Magnetic Materials and Integrated Circuits, Northeastern University, Boston, Massachusetts

Correspondence
Gang Wang and Dainan Zhang, State Key Laboratory of Electronic Thin Films and Integrated Devices, University of Electronic Science and Technology of China, Chengdu 610054, China.
Email: wang_toward@163.com (G. W.); dnzhang@uestc.edu.cn (D. Z.)

Funding information
National Key Scientific Instrument and Equipment Development Project, Grant/Award Number: 51827802; National Key Research and Development Plan, Grant/Award Number: 2016YFA0300801; National High-Tech Research and Development Program of China, Grant/Award Number: 2015AA034102; National Natural Science Foundation of China, Grant/Award Numbers: 51402041, 51602036 and 51672036

Abstract

Composition and structure play dominant roles in realizing the microwave dielectric properties that are necessary for the ever-increasing demands of the Internet of Things and related communication technologies. In the present study, the substitution of Ta^{5+} in $Li_3Mg_2Nb_{1-x}Ta_xO_6$ ceramics and its effect on the structural characteristics and microwave dielectric performances is systematically studied. All the substituted compositions were determined to be pure phase orthorhombic Li3Mg2NbO6 structure of space group *Fddd*. Furthermore, a NbO_6 octahedral distortion, Nb-O bond valence, packing fraction and polarizability were calculated to explore the structure-property-performance paradigm in the context of microwave dielectric performance. Scanning electron microscopy revealed homogeneous microstructures, with the introduction of Ta^{5+} promoting grain growth. Raman spectra indicated that the variation of the band (blue shift and red shift) at 771 cm^{-1} was highly correlated with the variation in unit cell volume. The polarizability significantly impacted ε_r values. The $Q \times f$ values were strongly influenced by the packing fraction and grain size. The changes in the NbO_6 octahedral distortion and Nb–O bond valence impacted the τ_f values. The $Li_3Mg_2Nb_{0.98}Ta_{0.02}O_6$ composition displayed the most dramatic improvements in microwave dielectric properties: $\varepsilon_r = 15.58$, $Q \times f = 113\,000$ GHz and $\tau_f = -4.5$ ppm/°C, providing a potential candidate for next generation microwave and millimeter-wave applications.

KEYWORDS

$Li_3Mg_2Nb_{1-x}Ta_xO_6$ ceramics, microwave properties, millimeter-wave properties, orthorhombic structure, structural characterization

1 | INTRODUCTION

In recent years, dielectric materials have been widely researched to address the demand for passive devices, such as filters, capacitors, dielectric resonators, and functional substrates.[1–4] In order to increase the propagation velocity and inhibit signal damping, dielectric materials should possess high quality factor and permittivity.[5–8] For practical engineering applications, the temperature coefficient of resonance frequency must be close to zero to guarantee the stability of performance.[9,10] However, many types of dielectric ceramics do not possess these properties. Instead, materials with high dielectric loss or large temperature coefficients of resonance frequency are quite common. Therefore, how to improve the

dielectric properties remains a central tenant of materials research and design efforts for microwave engineering applications.[11–15] In order to obtain the desired dielectric materials, a theory relating structure and microwave dielectric properties has been proposed.[12,16–19]

Recently, ceramic materials containing lithium having a rock-salt structure possess unique potential for practical applications due to suitable microwave dielectric properties.[20] Bian et al have researched the dielectric performance of $Li_3Mg_2NbO_6$ ceramics and discussed the structural evolution using X-ray diffractometry, infrared reflectivity, and Raman spectroscopy.[21] In order to modify the microwave dielectric performance, Zuo et al employed the introduction of Zn^{2+} ions for Mg^{2+}, which greatly improved the $Q \times f$ values for $Li_3Mg_2NbO_6$ ceramics.[15] Additionally, Zhang et al adopted the concomitant introduction of strategic ion substitution and glass additives to modify the microwave dielectric properties.[22–26] However, these measurements did not show any significant effect on τ_f values. In order to obtain a desirable near-zero τ_f value, some structural characteristics were calculated to establish the relationship between the structure and dielectric performance.[27,28] In a previous work, these authors determined the dielectric performance of $Ni_{0.5}Ti_{0.5}Nb_{1-x}Ta_xO_4$ ceramics.[29] Notably, the ionic radii of Ta^{5+} (0.64 Å) and Nb^{5+} (0.64 Å) are identical and therefore solid solutions are readily formed for low level cation substitutions. Alternatively, tantalum-containing materials usually have different crystal structures as compared to niobium-containing materials, hence, even low level substitutions of Ta^{5+} cations may perturb the structure of the parent compound and its microwave dielectric performance.

According to previous studies, τ_f values of $Li_3Mg_2NbO_6$ ceramics can be tuned to near-zero by employing limited substitutions.[30,31] In the present study, a near-zero τ_f was obtained for the composition having $x = 0.02$. Additionally, the $Q \times f$ values first increase, reaching a maximum for $x = 0.03$, and then decrease, which indicates that a higher Ta^{5+} substitution content of $x > 0.04$ does not exhibit any significant contribution to improving $Q \times f$ values. The melting temperature of Ta_2O_5, that is, 1800°C, is substantially higher than that of Nb_2O_5 i.e., 1480°C, and therefore, the sintering temperatures of samples having high Ta^{5+} content are expected to be higher than that of $Li_3Mg_2NbO_6$ ceramics. The troublesome evaporation of lithium occurs in $Li_3Mg_2NbO_6$ ceramics above 900°C, which is detrimental to the microwave dielectric properties.[19] High-temperature sintered $Li_3Mg_2(Nb_{1-x}Ta_x)O_6$ ceramics therefore will suffer from considerable evaporation of lithium, resulting in a porous microstructure with limited application value. Due to these reasons, a limited range of substitutions has been investigated. The impact of the substitution of Ta^{5+} ions on enhancing the microwave dielectric properties and relating these properties to crystal structure are discussed. Structural characterization, including the measurement of octahedra distortion, Nb-O bond valence, polarizability and packing fraction were determined using Rietveld refinement.

2 | EXPERIMENTAL PROCEDURES

2.1 | Materials preparation

New, low-loss $Li_3Mg_2Nb_{1-x}Ta_xO_6$ ceramics were fabricated using the solid-state reaction process. High-purity starting materials of Li_2CO_3, Nb_2O_5, Ta_2O_5, and MgO (phase purities >99%) were employed. The chemicals were weighed adhering to the nominal stoichiometric ratios of the $Li_3Mg_2Nb_{1-x}Ta_xO_6$ compounds. The raw materials were mixed and ball-milled for 4 h. The processed powders were calcined at 1025°C in an alumina crucible for 4 h to compare with results of a previous study.[27] According to Wu and Kim,[19] minor evaporation of lithium occurs upon sintering at temperatures at ~1000°C. As a precaution, after calcination the surfaces exposed to air were removed. The remaining calcined powders were milled for another 4 h and pressed into cylindrical disks (i.e., pellets). These pellets were then surrounded by free powder of the same composition to provide a Li-rich local atmosphere and prevent exposure to the reactive atmosphere. These powders and pellets were then sintered from 1050 to 1150 for 4 h.

2.2 | Characterization

The phase purity of samples was analyzed using X-ray $\theta-2\theta$ powder diffraction employing an X-ray diffractometer (Philips X'pert Pro MPD) at room temperature using Cu-Kα radiation ($\lambda = 0.1542$ nm). The 2θ angles were measured from 10° to 120° with a step size of 0.02°. Rietveld refinement of measured $\theta-2\theta$ data were employed using the EXPGUI software suite.[32] Raman spectroscopy (InVia, Renishaw) was used to investigate the variations in crystal structure of $Li_3Mg_2Nb_{1-x}Ta_xO_6$ samples, where $x = 0$, 0.01, 0.02, 0.03, and 0.04. The microstructure and morphology were analyzed using scanning electron microscopy (SEM; JEOL, JSM-6490). SEM micrographs were measured to obtain robust statistical analyses of grain sizes, as shown in Figure S1. For each composition, the analyzed sample area consisted of approximately 100 grains and the grain size distributions were obtained using Image-Pro Plus. The bulk densities were measured using Archimedes method. The relative permittivity and $Q \times f$ values were calculated using the Hakki-Coleman method utilizing a network analyzer (Agilent, N5230A) over a frequency range of 9-12 GHz. A silver-coated cylindrical resonance cavity using a sample diameter-to-height ratio of approximately 2, where samples were placed in the center of the cavity, was employed. The unloaded Q-factor was determined using Equation 1.

$$Q = \frac{Q_L}{1 - 10^{-IL_0/20}} \quad (1)$$

where Q_L is the loaded quality factor and can be calculated from the 3 dB full width of the resonance peak. Additionally, IL_0 (dB) is the insertion loss, equal to the absolute value of S_{21} (dB). In order to prevent coupling the S_{21} parameter was adjusted to a value of less than −50 dB. The total uncertainty of permittivity did not exceed 0.3% and the deviation of $Q \times f$ value did not exceed 3%. The τ_f values were determined according to the resonant frequency at temperatures of 25 and 85°C using Equation 2.

$$\tau_f = \frac{f_{85} - f_{25}}{f_{25} \times 60} \times 10^6 (\text{ppm}/^\circ\text{C}) \quad (2)$$

3 | RESULTS AND DISCUSSION

3.1 | Phase identification and composition

Figure 1 shows the XRD patterns of $Li_3Mg_2Nb_{1-x}Ta_xO_6$ ($x = 0$, 0.01, 0.02, 0.03 and 0.04) ceramics sintered at 1100°C. The standard diffraction patterns, extracted from PDF card 86-0346, is provided and the crystallographic planes of all diffraction peaks for the experimental data are indexed. No secondary phases were detected above the detection limit of the instrument for all samples, indicating that the Ta^{5+} ions likely diffused into the lattice as substitute ions for the Nb^{5+} ions. This result is consistent with Ta^{5+} ions having the same ionic radius (0.64 Å) as that of Nb^{5+} ion (0.64 Å). According to Goldschmidt's rule, the difference in ionic radii (ΔR) for ionic substitution is given by Equation 3.[33]

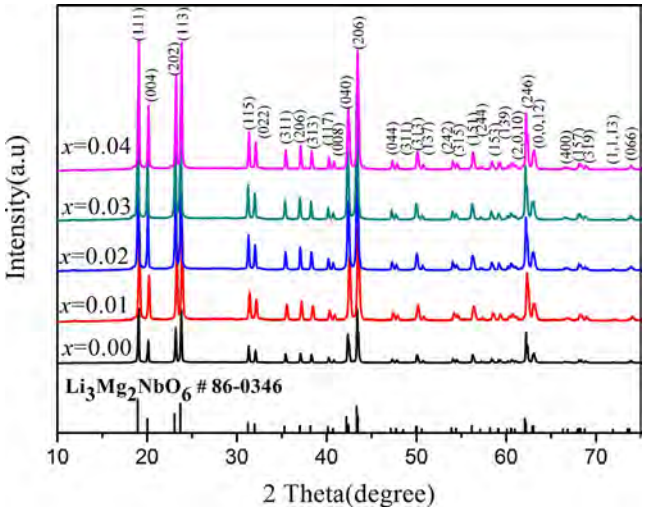

FIGURE 1 XRD diffraction patterns of $Li_3Mg_2Nb_{1-x}Ta_xO_6$ ($x = 0$–0.04) ceramics sintered at 1100°C

$$\Delta R = \frac{R_{Ta} - R_{Nb}}{R_{Nb}} \quad (3)$$

Accordingly, if ΔR is less than 15%, a solid solution is expected. Ringwood et al also investigated the substitution rules based upon electronegativity and found that the difference in electronegativity is about 0.1 in most of the cases involving substitution.[34] In the present work, ΔR and the difference in electronegativity between Ta^{5+} ions and Nb^{5+} ion are 0 and 0.1, respectively. Additionally, unit cell parameters varied due to the possible evaporation of lithium and differences in electronegativity of Ta^{5+} and Nb^{5+} ions, as presented in Table 1.

Figure 2 shows a schematic of the $Li_3Mg_2NbO_6$ unit cell with orthorhombic structure and Rietveld refinements of $Li_3Mg_2Nb_{1-x}Ta_xO_6$ ($x = 0$, 0.01, 0.02, 0.03, and 0.04) compositions sintered at 1100°C. As exhibited in Figure 2A, each primitive unit cell consists of eight $Li_3Mg_2NbO_6$ formula units. Nb^{5+} cations occupy one set of octahedral sites, while Li/Mg cations randomly occupy the other three octahedral sites. Li/Nb/Mg cations are linked to six oxygen atoms to form an oxygen octahedron.[35] Adopting $Li_3Mg_2NbO_6$ as the initial model, Rietveld refinements were conducted using the EXPGUI software for all the compositions. Figure 2A-F present the refinement patterns of $Li_3Mg_2Nb_{1-x}Ta_xO_6$ ($x = 0$, 0.01, 0.02, 0.03, and 0.04) compositions sintered at 1100°C. The results showed that the calculated patterns are consistent with the measured data and the R_p values are less than 6%, whereas the R_{wp} values are less than 7%, indicating that the structural models for Rietveld refinements are reliable. The structural parameters of $Li_3Mg_2Nb_{1-x}Ta_xO_6$ ceramics for Rietveld refinement are presented in Table S1. The Rietveld refinement parameters, including the reliability

TABLE 1 Lattice parameters, unit cell volume and the reliability factors of $Li_3Mg_2Nb_{1-x}Ta_xO_6$ ($x = 0$, 0.01, 0.02, 0.03, and 0.04) ceramics sintered at 1100°C

x	0.00	0.01	0.02	0.03	0.04
a (Å)	5.9019	5.9003	5.8986	5.8969	5.8970
b (Å)	8.5455	8.5446	8.54233	8.5417	8.5476
c (Å)	17.7388	17.7346	17.73231	17.7251	17.7232
V (Å^3)	894.6371	894.110	893.998	893.7103	893.951
R_p (%)	5.2	3.53	4.97	4.32	5.01
R_{wp} (%)	7.0	4.82	6.95	5.87	6.91
χ^2	2.2	2.6	3.7	2.9	4

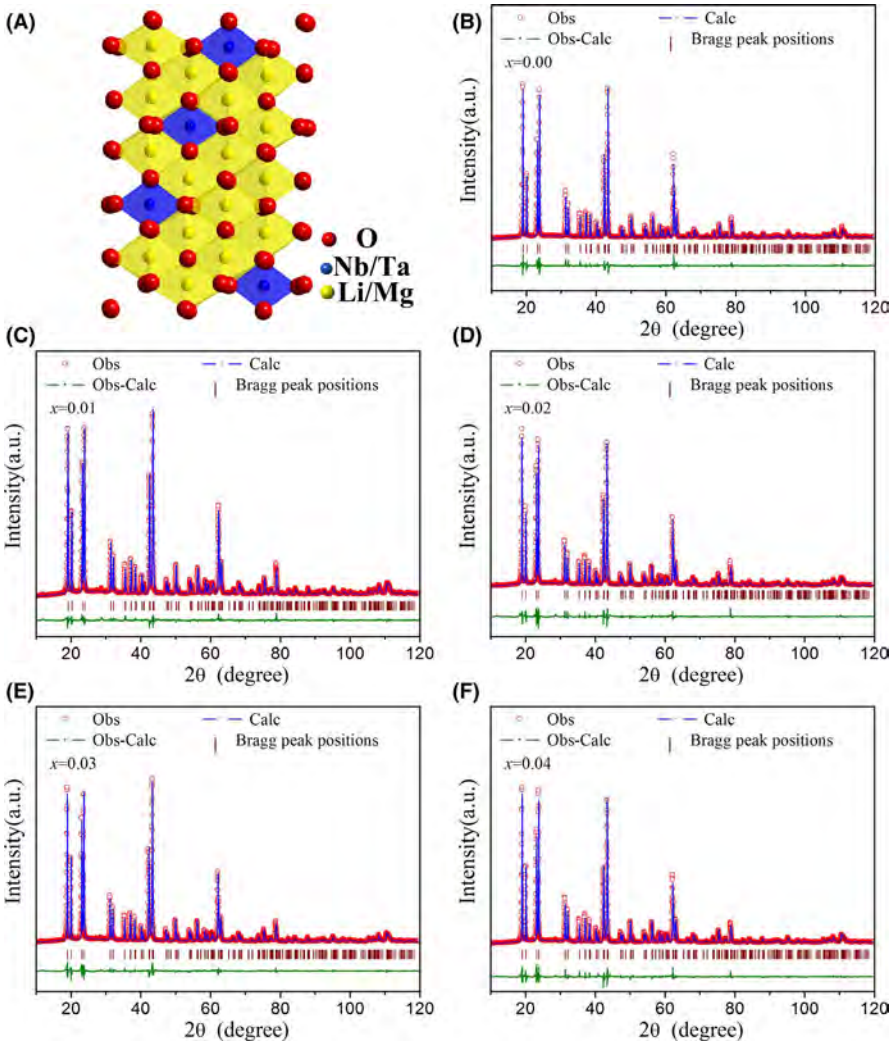

FIGURE 2 Crystal structure for $Li_3Mg_2NbO_6$ ceramics (A) and Rietveld refinement patterns for $Li_3Mg_2Nb_{1-x}Ta_xO_6$ (x = 0–0.04) ceramics, (B) x = 0, (C) x = 0.01, (D) x = 0.02, (E) x = 0.03 and (F) x = 0.04

factors (χ^2, R_{wp}, and R_p), lattice constant and unit cell volume of $Li_3Mg_2Nb_{1-x}Ta_xO_6$ (x = 0, 0.01, 0.02, 0.03, and 0.04) ceramics are listed in Table 1.

3.2 | Structural analysis

It is well known that crystal structure plays a dominant role in determining microwave dielectric properties.[4,36] Therefore, it is essential to quantify Nb-O bonds and lattice vibrations in order to better understand the origins of microwave dielectric properties. These were investigated using Raman spectroscopy and Rietveld refinements. Due to the substitution of Nb^{5+} ions by Ta^{5+}, the crystal structure of $Li_3Mg_2NbO_6$ become slightly distorted, which may modify the microwave dielectric properties. The Nb-site bond valence and NbO_6 octahedral distortions were calculated using Rietveld refinement. The NbO_6 octahedral distortion was calculated using Equation 4.[37]

$$\delta = \frac{1}{6}\sum\left(\frac{R_i - \overline{R}}{\overline{R}}\right)^2 \quad (4)$$

where $\overline{R}$ and R_i are the average and individual bond lengths of Nb-O bonds, respectively. The bond valence V_{ij} (atom i) was determined using Equations 5 and 6.

$$V_{ij} = \sum v_{ij} \quad (5)$$

$$v_{ij} = \exp\left(\frac{R_{ij} - d_{ij}}{b}\right) \quad (6)$$

where R_{ij} represents the bond valence, b is a constant (0.37 Å) and d_{ij} indicates the bond length between atoms i and j. The bond valence parameter R_{NbO} is 1.911 Å.[38] The calculated results are listed in Table 2. The differences in NbO_6 octahedral distortion and Nb–O bond valence are attributed to the lower electronegativity of Ta^{5+} ion compared with that of the Nb^{5+} ion. The NbO_6 octahedral distortion and Nb-O bond valence were calculated to explore the dependence of τ_f values on structural properties.

TABLE 2 Bond lengths, Nb-site bond valence and distortion of NbO_6 octahedron of $Li_3Mg_2Nb_{1-x}Ta_xO_6$ ($x = 0$, 0.01, 0.02, 0.03, and 0.04) ceramics sintered at 1100°C

x	Bond	$d_{Nb\text{-}O}$	$v_{Nb\text{-}O}$	$V_{Nb\text{-}O}$	$\overline{R}$	δ	τ_f (ppm/°C)
0.00	Nb-O(1) × 2	1.9579	0.8810	4.8324	1.9919	1.46×10^{-4}	−17
	Nb-O(2) × 4	2.0089	0.7676				
0.01	Nb-O(1) × 2	1.9569	0.8833	4.8228	1.9927	1.61×10^{-4}	−12.5
	Nb-O(2) × 4	2.0106	0.7640				
0.02	Nb-O(1) × 2	1.9585	0.8795	4.7805	1.9960	1.77×10^{-4}	−4.5
	Nb-O(2) × 4	2.0148	0.7554				
0.03	Nb-O(1) × 2	1.9598	0.8764	4.7785	1.9959	1.66×10^{-4}	−7.1
	Nb-O(2) × 4	2.0143	0.7564				
0.04	Nb-O(1) × 2	1.9574	0.8821	4.8153	1.9933	1.62×10^{-4}	−14.3
	Nb-O(2) × 4	2.0112	0.7527				

Raman spectroscopy is extremely sensitive to local structure. In the present work, Raman spectroscopy is adopted to investigate modifications of crystal structure for $Li_3Mg_2Nb_{1-x}Ta_xO_6$ ceramics. According to the space group *Fddd* and symmetry analysis, the optical models are provided by the Bilbao Crystallographic Server[39] (see Equation 7).

$$\Gamma_{Raman} = 8A_g + 12B_{1g} + 15B_{2g} + 16B_{3g} \quad (7)$$

The factor group analysis exhibited that 51 Raman active vibrational modes exist in the $Li_3Mg_2NbO_6$ crystal structure. Due to the interaction or overlapping modes, the observed Raman spectra consisted of less vibrations than the theoretical model. As shown in Figure 3, all the compositions explored here possessed similar Raman spectra. The bands around 155 cm^{-1} are correlated to Nb bond vibrations, while the bands within the 250–450 cm^{-1} were assigned to Li–O bond stretching vibrations according to studies of the Li_2SiO_3 and $Li_{(3-3x)}M_{4x}Nb_{(1-x)}O_4$ systems.[21,40] The band at around 477 cm^{-1} may be attributed to Nb-Nb stretching, while the band at around 771 cm^{-1} was assigned to Mg-O bond vibrations.[41] Notably, the band at 771 cm^{-1} was at first shifted to a higher wavenumber, and then, to a lower wavenumber, which was highly correlated to the variation in unit cell volume.[42]

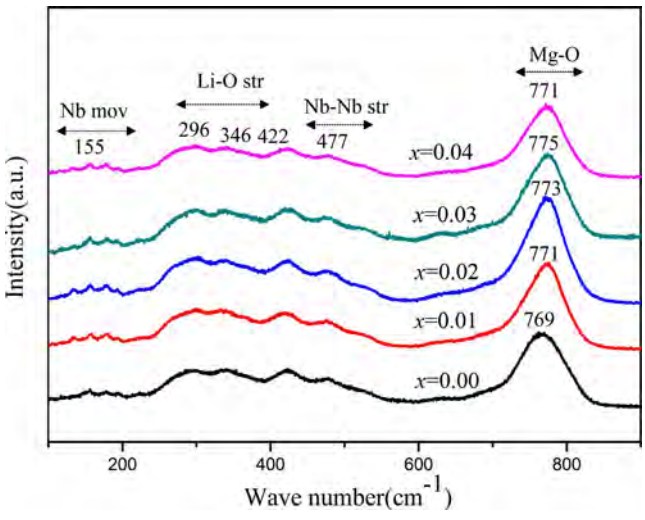

FIGURE 3 Raman spectra of the $Li_3Mg_2Nb_{1-x}Ta_xO_6$ ($x = 0$–0.04) ceramic

3.3 | Microstructure analysis

Figure 4 shows the SEM micrographs of $Li_3Mg_2Nb_{1-x}Ta_xO_6$ (x = 0, 0.01, 0.02, 0.03, and 0.04) samples. In the present work, the morphology, porosity and grain size were related to the compositions and dopant levels. The grain boundaries and dense microstructure were clearly observed for all sintered samples. As the content of Ta^{5+} increased, the densification and average grain size first increased, and at higher doping levels, decreased. For $x \leq 0.01$, a porous microstructure was detected with an average grain size of around 9 μm. For $0.02 \leq x \leq 0.03$, denser and more homogeneous microstructures were observed. Furthermore, the average grain size reached a maximum of about 12 μm. For the sample with $x = 0.04$, the grain size decreased to 10.68 μm. These results indicate that suitable levels of Ta^{5+} substitutions promote grain growth and improve the density of $Li_3Mg_2Nb_{1-x}Ta_xO_6$ ceramics. In comparison, for $x = 0.03$, the sintered samples presented inhomogeneous microstructure with some relatively small grains. In comparison of SEM images, 1100°C was found to be the optimal sintering temperature. According to previous work, it is well known that grain boundaries contribute significantly to dielectric loss by acting as two-dimensional defects.[43,44] The increase in average grain size translates to a decrease in grain boundary density. Therefore, the grain size plays a key role in determining microwave

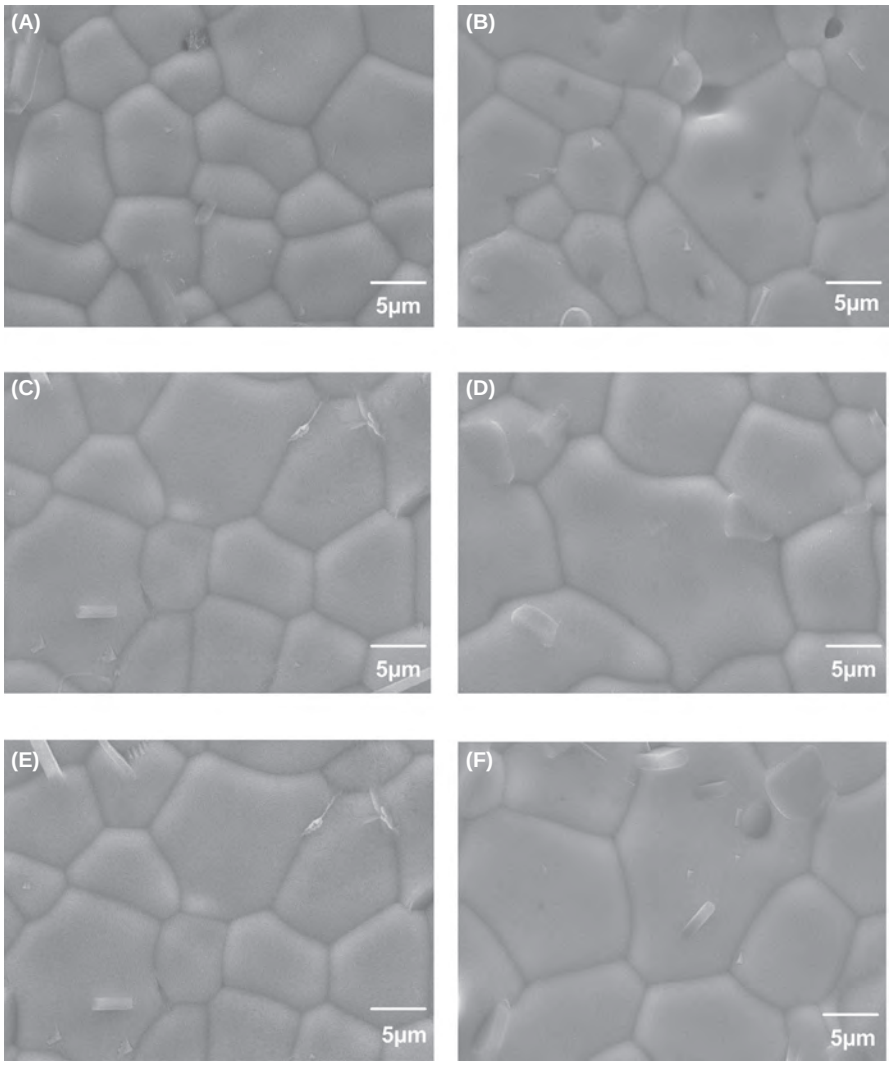

FIGURE 4 Surface SEM micrographs of $Li_3Mg_2Nb_{1-x}Ta_xO_6$ ceramics sintered at 1100°C (A) $x = 0$, (B) $x = 0.01$, (C) $x = 0.02$, (D) $x = 0.03$, (E) $x = 0.04$ and (F) $x = 0.03$ sintered at 1125°C

dielectric properties. The distribution of grain size and average grain size of $Li_3Mg_2Nb_{1-x}Ta_xO_6$ ceramics sintered at 1100°C are shown in Figure S2. With the Ta^{5+} content reaching $x = 0.03$, the distribution of small grains vanishes and grain boundaries decreases, which improves $Q \times f$ values. The measured average grain sizes were 9.36, 10.37, 10.71, 13.65, and 12.02 μm for $x = 0$, 0.01, 0.02, 0.03, and 0.04, respectively. These results support that suitable Ta^{5+} substitution promotes grain growth.

3.4 | Dielectric property analysis

Figure 5 presents the relative permittivity of $Li_3Mg_2Nb_{1-x}Ta_xO_6$ ($x = 0$, 0.01, 0.02, 0.03, and 0.04) ceramics for various sintering temperatures and Ta^{5+} substitution. Ordinarily, the relative permittivity is dependent on many factors, such as ionic polarizability, second phases and density.[45] In this study, the relative permittivity of all substitutional compositions increased (and then reduced) with the increase in sintering temperature, which was related to the relative density and polarizability. Figures 1 and 2 show a single orthorhombic structure. Therefore, the effects of secondary phases on the dielectric constant is eliminated. The relationship among relative permittivity, relative density and polarizability can be described using the Clausius-Mosotti equation[6] (see Equation 8).

$$\frac{\varepsilon_r - 1}{\varepsilon_r + 2} = \frac{N\alpha}{3\varepsilon_0} \tag{8}$$

where α, ε_0, and ε_r are the molecular polarizability, permittivity of the vacuum and dielectric ceramics, respectively. As the substituting Ta^{5+} content increased, the dielectric constant of as-sintered samples sintered at 1100°C increased, which can be attributed to higher ionic polarizability of Ta^{5+} (4.73 Å) than that of Nb^{5+} (3.97 Å). The theoretical dielectric polarizability (α_{theo}) of $Li_3Mg_2Nb_{1-x}Ta_xO_6$ ceramics was obtained using the Shannon's additive rule[46] (see Equation 9).

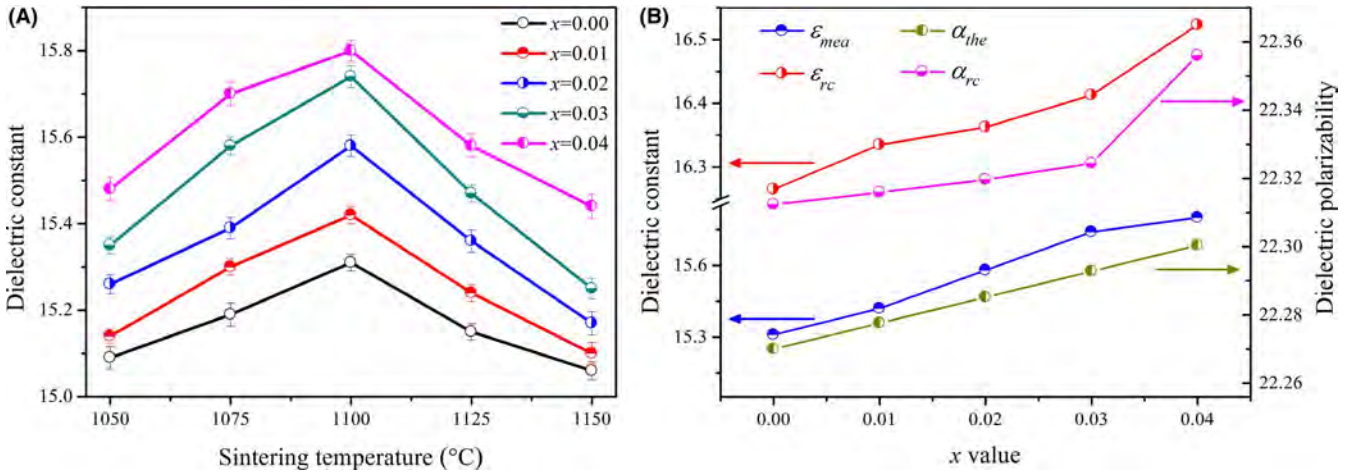

FIGURE 5 Variation in dielectric constant of $Li_3Mg_2Nb_{1-x}Ta_xO_6$ ceramics with temperature (A), and dielectric constant of the ceramics sintered at 1100°C for various values of polarizability (B)

$$\alpha_{theo} = 3\alpha\left(Li^{+}\right) + 2\alpha\left(Mg^{2+}\right) + (1-x)\,\alpha\left(Nb^{5+}\right) + x\alpha\left(Ta^{5+}\right) + 6\alpha\left(O^{2-}\right) \quad (9)$$

where α (Ta^{5+}) = 4.37 Å^3, α (Nb^{5+}) = 3.97 Å^3, α (Mg^{2+}) = 1.32 Å^3, α (O^{2-}) = 2.01 Å^{3}and α (Li^{+}) = 1.20 Å^3 are the ionic polarizabilities. In order to eliminate the impact of porosity on permittivity, permittivity was corrected using Equation 10.[47]

$$\varepsilon_{mea} = \varepsilon_{rc}\left(1 - \frac{3p\left(\varepsilon_{rc}-1\right)}{2\varepsilon_{rc}+1}\right) \quad (10)$$

where p, ε_{mea}, and ε_{rc} are the porosity fraction, measured permittivity and porosity-corrected permittivity, respectively. In order to determine the porosity fraction, the theoretical density, calculated based on the results of refinement, was determined to be approximately 3.84 g/cm^3. The observed dielectric polarizability (α_{obs}) was obtained using the abovementioned porosity-corrected permittivity[48,49] (see Equation 11).

$$\alpha_{rc} = \frac{V_m}{b}\frac{(\varepsilon_{rc}-1)}{(\varepsilon_{rc}+2)} \quad (11)$$

where b and V_m are the constant ($4\pi/3$) and the molar volume, respectively. Table 3 summarizes the results for ε_{mea}, ε_{rc}, ε_{theo}, α_{theo}, and α_{obs} of $Li_3Mg_2Nb_{1-x}Ta_xO_6$ ceramics sintered at 1100°C. As the substituting Ta^{5+} content increased, the porosity-corrected permittivity increased. The porosity-corrected dielectric polarizability increased with the increase in the substituting Ta^{5+} content, showing the same variation trend with theoretical dielectric polarizability. Based on Equations 9 and 11, the theoretical permittivity was calculated and presented in Table 3. Remarkably, an extremely small discrepancy of ($\Delta = |(\alpha_{theo} - \alpha_{rc})/\alpha_{rc} \times 100\%| \leq 1\%$ existed among all the compositions, indicating that the calculated α_{obs} values were in close agreement with α_{theo} values. Additionally, a larger difference (5.1%) between the measured and theoretical permittivities was obtained. It is interesting that the porosity-corrected permittivity was larger than the theoretical permittivity, which is possibly related to polyhedral distortions and atomic vibrations, as reported in previous works.[4,50]

Figure 6 presents the $Q \times f$ values of $Li_3Mg_2Nb_{1-x}Ta_xO_6$ (x = 0, 0.01, 0.02, 0.03, and 0.04) ceramics for different sintering temperatures and substituting Ta^{5+} contents. With the increase in sintering temperature, the $Q \times f$ values first increased, and then, decreased for all compositions. It is well known that the $Q \times f$ values are affected by many factors, including structural properties, grain size, secondary phases and density.[4,36] Therefore, the packing fraction was calculated to investigate its impact on $Q \times f$ values[50] (see Equation 12).

$$\text{Packing fraction} = \frac{\text{volume of the atoms in the cell}}{\text{volume of unit cell}} \times Z \quad (12)$$

TABLE 3 Measured dielectric constant (ε_{mea}), porosity-corrected dielectric constant (ε_{rc}), theoretical dielectric constants (ε_{theo}), observed dielectric polarizabilities (α_{obs}) and theoretical dielectric polarizabilities (α_{theo}) values of $Li_3Mg_2Nb_{1-x}Ta_xO_6$ (x = 0, 0.01, 0.02, 0.03 and 0.04) ceramics sintered at 1100°C

x	0.00	0.01	0.02	0.03	0.04
p (%)	4.3	4.1	3.5	3	3.2
ε_{theo}	16.0903	16.1754	16.2184	16.2798	16.2865
ε_{mea}	15.31	15.42	15.58	15.74	15.8
ε_{rc}	16.2652	16.335	16.3626	16.4130	16.523
α_{rc}	22.3124	22.3159	22.3197	22.3244	22.356
α_{theo}	22.27	22.2776	22.2852	22.2928	22.3004
Δ (%)	0.19	0.173	0.154	0.142	0.249

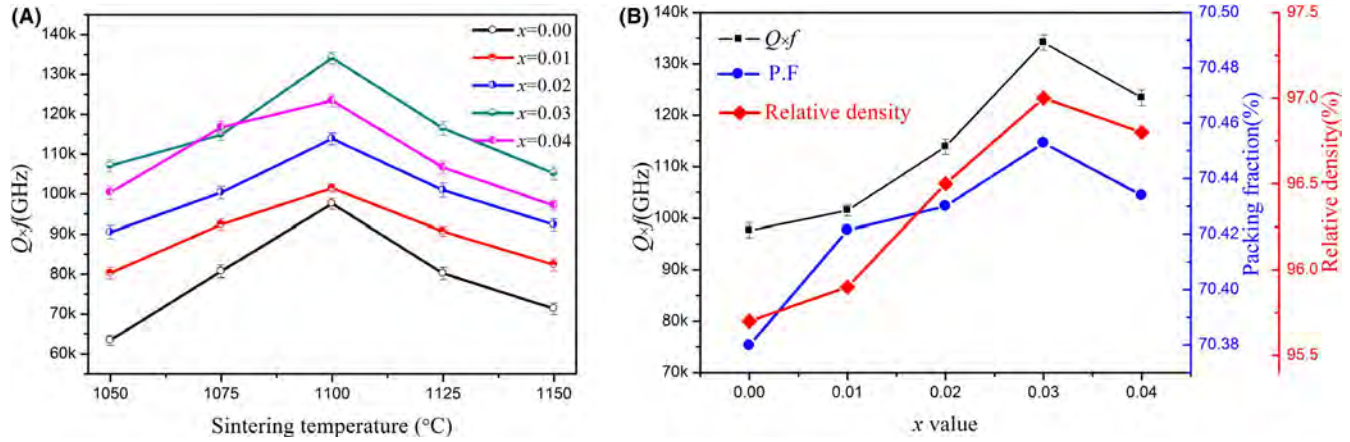

FIGURE 6 $Q \times f$ values of $Li_3Mg_2Nb_{1-x}Ta_xO_6$ ($x = 0$–0.04) ceramics at various temperatures (A), and $Q \times f$ values of the sample sintered at 1100°C for various packing fractions (B)

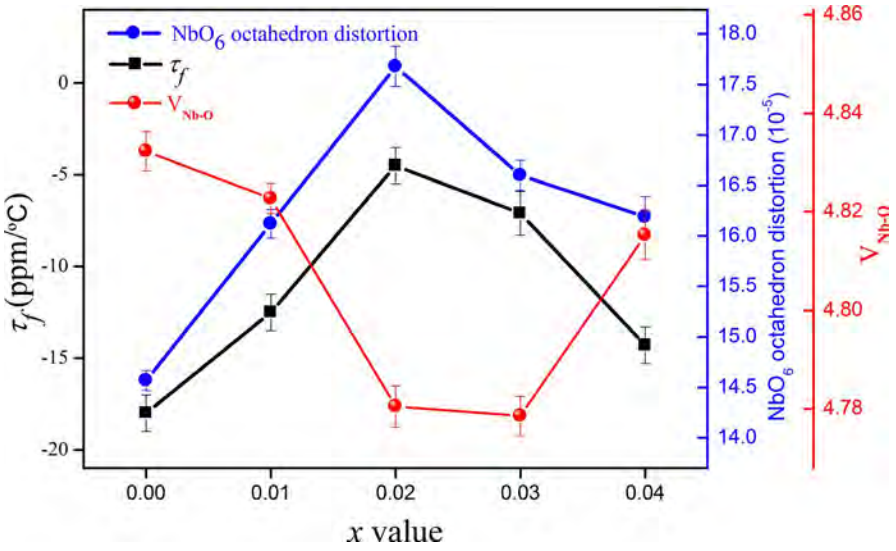

FIGURE 7 τ_f values and NbO_6 octahedron distortions for $Li_3Mg_2Nb_{1-x}Ta_xO_6$ ($x = 0$–0.04) ceramics sintered at 1100°C

where Z is 8 for $Li_3Mg_2NbO_6$ ceramics. The calculated results are listed in Table S2. Figure 6B presents the relationship among $Q \times f$ values, packing fractions and relative densities. The $Q \times f$ values increased, and then decreased, which is similar to trends in relative densities and packing fractions. However, the relative density was higher than 95%, indicating the density may be correlated but may not have a causal relationship with $Q \times f$ values. Additionally, the trend in average grain size is similar to that of $Q \times f$ values, as shown in Table S2. Therefore, it is implied that $Q \times f$ values are dependent on the packing fraction and grain size.

Figure 7 exhibits τ_f values and NbO_6 octahedral distortion of $Li_3Mg_2Nb_{1-x}Ta_xO_6$ ($x = 0$, 0.01, 0.02, 0.03, and 0.04) ceramics. Generally, τ_f is correlated with the temperature coefficient of the dielectric constant (τ_ε) following Equation 13.

$$\tau_f = -\alpha - \frac{1}{2}\tau_\varepsilon \tag{13}$$

The τ_ε values are affected by structural properties including octahedral distortions and Nb-O bond valence. With the increase in the content of Ta^{5+}, the τ_f values increased and then decreased, which is attributed to the NbO_6 octahedral distortion and Nb-O bond valence.

4 | CONCLUSIONS

In the present work, low-loss $Li_3Mg_2Nb_{1-x}Ta_xO_6$ ($x = 0$, 0.01, 0.02, 0.03, and 0.04) ceramics were fabricated using the solid-state reaction process. The impact of Ta^{5+} substitution on structural characteristic and the corresponding enhancement in the microwave dielectric properties were investigated. Based on Rietveld refinement results, all substituted compositions were indexed to a single orthorhombic Li3Mg2NbO6 phase. Additionally, homogeneous microstructures with uniform grain sizes (13.65 μm) were observed for the $Li_3Mg_2Nb_{1-x}Ta_xO_6$ ($x = 0.03$) composition. NbO_6

octahedral distortions, Nb-O bond valence, packing fraction and polarizability were measured and calculated to establish relationships between structural properties and microwave dielectric performance. Furthermore, an extremely small discrepancy between the values of α_{theo} and α_{rc} was observed and ε_r values were correlated to polarizability. The $Q \times f$ values were largely affected by the packing fraction and grain size. The τ_f values depended on NbO_6 octahedral distortions and Nb-O bond valence. In particular, the $Li_3Mg_2Nb_{1-x}Ta_xO_6$ ($x = 0.02$) composition exhibited substantial microwave dielectric enhancements: $\varepsilon_r = 15.58$, $Q \times f = 113\ 000$ GHz and $\tau_f = -4.5$ ppm/°C, which provides a promising candidate for microwave and millimeter-wave applications.

ACKNOWLEDGMENTS

This work was financially supported by the National Key Scientific Instrument and Equipment Development Project (grant no. 51827802), the National Key Research and Development Plan (grant no. 2016YFA0300801), the National High-Tech Research and Development Program of China (grant no. 2015AA034102), and the National Natural Science Foundation of China (Grant nos 51402041, 51602036 and 51672036).

ORCID

Gang Wang https://orcid.org/0000-0002-1708-0225
Fang Xu https://orcid.org/0000-0003-3126-532X
Yulong Liao https://orcid.org/0000-0003-1427-0717

REFERENCES

1. Fiedziuszko SJ, Hunter IC, Itoh T, Kobayashi Y, Nishikawa T, Stitzer SN, et al. Dielectric materials, devices, and circuits. IEEE Trans Microw Theory Tech. 2002;50(3):706–20.
2. Wersing W. Microwave ceramics for resonators and filters. Curr Opin Solid St M. 1996;1(5):715–31.
3. Reaney IM, Iddles D. Microwave dielectric ceramics for resonators and filters in mobile phone networks. J Am Ceram Soc. 2006;89(7):2063–72.
4. Fu Z, Liu P, Ma J, Zhao X, Zhang H. Novel series of ultra-low loss microwave dielectric ceramics: $Li_2Mg_3BO_6$ (B=Ti, Sn, Zr). J Eur Ceram Soc. 2016;36(3):625–9.
5. Sebastian MT, Jantunen H. Low loss dielectric materials for LTCC applications: a review. Int Mater Rev. 2008;53(2):57–90.
6. Maex K, Baklanov MR, Shamiryan D, Lacopi F, Brongersma SH, Yanovitskaya ZS. Low dielectric constant materials for microelectronics. J Appl Phys. 2003;93(11):8793–841.
7. Yao GG, Liu P, Zhang HW. Novel series of low-firing microwave dielectric ceramics: $Ca_5A_4(VO_4)_6$ (A^{2+}=Mg, Zn). J Am Ceram Soc. 2013;96(6):1691–3.
8. Guo J, Zhou D, Wang H, Yao X. Microwave dielectric properties of (1–x)$ZnMoO_4$-xTiO_2 composite ceramics. J Alloy Compd. 2011;509(19):5863–5.
9. Guo Q, Li L, Yu S, Sun Z, Zheng H, Li J, et al. Temperature–stable dielectrics based on Cu–doped $Bi_2Mg_{2/3}Nb_{4/3}O_7$ pyrochlore ceramics for LTCC. Ceram Int. 2018;44(1):333–8.
10. Wang G, Zhang H, Liu C, Su H, Li J, Huang X, et al. Low temperature sintering and microwave dielectric properties of novel temperature stable $Li_3Mg_2NbO_6$-0.1TiO_2 ceramics. Mater Lett. 2018;217:48–51.
11. Zhou D, Wang H, Pang LX, Yao X, Wu XG. Low temperature firing of $BiSbO_4$ microwave dielectric ceramic with B_2O_3-CuO addition. J Eur Ceram Soc. 2009;29(8):1543–6.
12. Zhou D, Li J, Pang L-X, Chen G-H, Qi Z-M, Wang D-W, et al. Crystal structure, infrared spectra, and microwave dielectric properties of temperature-stable zircon-type (Y, Bi)V_O4 solid-solution ceramics. ACS Omega. 2016;1(5):963–70.
13. Fu Z, Liu P, Ma J, Chen X, Zhang H. New high Q low-fired $Li_2Mg_3TiO_6$ microwave dielectric ceramics with rock salt structure. Mater Lett. 2016;164:436–9.
14. Zhou DI, Randall CA, Pang L-X, Wang H, Guo J, Zhang G-Q, et al. Microwave dielectric properties of Li_2WO_4 ceramic with ultra-low sintering temperature. J Am Ceram Soc. 2011;94(2):348–50.
15. Zhang T, Zuo R. Effect of Li_2O–V_2O_5 addition on the sintering behavior and microwave dielectric properties of $Li_3(Mg_{1-x}Zn_x)_2NbO_6$ ceramics. Ceram Int. 2014;40(10, Part A):15677–84.
16. Wang G, Zhang H, Huang X, Xu F, Gan G, Yang Y, et al. Correlations between the structural characteristics and enhanced microwave dielectric properties of V–modified $Li_3Mg_2NbO_6$ ceramics. Ceram Int. 2018;44(16):19295–300.
17. Wu H, Kim ES. Correlations between crystal structure and dielectric properties of high-Q materials in rock-salt structure Li_2O-MgO-BO_2 (B = Ti, Sn, Zr) systems at microwave frequency. RSC Advances. 2016;6(53):47443–53.
18. Zhang P, Zhao YG, Li LX. The correlations among bond ionicity, lattice energy and microwave dielectric properties of $(Nd_{1-x}La_x)NbO_4$ ceramics. Phys Chem Chem Phys. 2015;17(26):16692–8.
19. Wu H, Kim ES. Characterization of low loss microwave dielectric materials $Li_3Mg_2NbO_6$ based on the chemical bond theory. J Alloy Compd. 2016;669:134–40.
20. Yuan LL, Bian JJ. Microwave dielectric properties of the lithium containing compounds with rock salt structure. Ferroelectrics. 2009;387:123–9.
21. Bian J, Liang Z, Wang L. Structural evolution and microwave dielectric properties of $Li_{(3-3x)}M_{4x}Nb_{(1-x)}O_4$ (M=Mg, Zn; 0≤x≤0.9). J Am Ceram Soc. 2011;94(5):1447–53.
22. Zhao Y, Zhang P. Microstructure and microwave dielectric properties of low loss materials $Li_3(Mg_{0.95}A_{0.05})_2NbO_6$ (A=Ca^{2+}, Ni^{2+}, Zn^{2+}, Mn^{2+}) with rock-salt structure. J Alloy Compd. 2016;658:744–8.
23. Zhang P, Xie H, Zhao Y, Zhao X, Xiao M. Low temperature sintering and microwave dielectric properties of $Li_3Mg2NbO_6$ ceramics doped with Li_2O–B_2O_3–SiO_2 glass. J Alloy Compd. 2017;690:688–91.
24. Zhang P, Liu L, Zhao Y, Xiao M. Low temperature sintering and microwave dielectric properties of $Li_3Mg_2NbO_6$ ceramics for LTCC application. J Mater Sci- Mater El. 2017;28(8):5802–6.
25. Zhang P, Liao JW, Zhao YG, Zhao XY, Xiao M. Effects of B_2O_3 addition on the sintering behavior and microwave dielectric properties of $Li_3Mg_2NbO_6$ ceramics. J Mater Sci-Mater El. 2017;28(1):686–90.

26. Zhang P, Zhao XY, Zhao YG. Effects of MBS addition on the low temperature sintering and microwave dielectric properties of $Li_3Mg_2NbO_6$ ceramics. J Mater Sci- Mater El. 2016;27(6):6395–8.
27. Wang G, Zhang H, Xu F, Huang X, Lai Y, Gan G, et al. Investigation and characterization on crystal structure and enhanced microwave dielectric properties of non-stoichiometric $Li_{3+x}Mg_2NbO_6$ ceramics. Ceram Int. 2018;44(16):20539–44.
28. Zhang P, Wu SX, Xiao M. Effect of Sb^{5+} ion substitution for Nb^{5+} on crystal structure and microwave dielectric properties for $Li_3Mg_2NbO_6$ ceramics. J Alloy Compd. 2018;766:498–505.
29. Huang X, Zhang HW, Lai YM, Wang G, Li MM, Hong CY, et al. Relationship of crystal structure and microwave dielectric properties in $Ni_{0.5}Ti_{0.5}NbO_4$ ceramics with Ta substitution. Eur J Inorg Chem. 2018;17:1800–4.
30. Xing CF, Bi JX, Wu HT. Effect of Co-substitution on microwave dielectric properties of $Li_3(Mg_{1-x}Co_x)_2NbO_6$ ($0.00 \le x \le 0.10$) ceramics. J Alloy Compd. 2017;719:58–62.
31. Wang G, Zhang H, Huang X, Xu F, Lai Y, Gan G, et al. Crystal structure and enhanced microwave dielectric properties of non-stoichiometric $Li_3Mg_{2+x}NbO_6$ ceramics. Mater Lett. 2019;235:84–7.
32. Toby BH. EXPGUI, a graphical user interface for GSAS. J Appl Crystallogr. 2001;34:210–3.
33. Goldschmidt VM. Die Gesetze der Krystallochemie. Naturwissenschaften. 1926;14(21):477–85.
34. Ringwood AE. The principles governing trace element distribution during magmatic crystallization Part I: The influence of electronegativity. Geochimt Cosmochim Acta. 1955;7(3):189–202.
35. Mather GC, Smith RI, Skakle J, Fletcher JG, Castellanos R, Gutierrez MP, et al. Synthesis and structures of the partially ordered rock salt phases, $Li_3M_2XO_6$: M=Mg Co, Ni; X=Nb, Ta. Sb. J Mater Chem. 1995;5(8):1177–82.
36. Kim ES, Chun BS, Freer R, Cernik RJ. Effects of packing fraction and bond valence on microwave dielectric properties of $A^{2+}B^{6+}O_4$ (A^{2+}: Ca, Pb, Ba; B^{6+}: Mo, W) ceramics. J Eur Ceram Soc. 2010;30(7):1731–6.
37. Li Y, Lu X, Zhang Y, Zou Y, Wang L, Zhu H, et al. Characterization of $Co_{0.5}(Ti_{1-x}Zr_x)_{0.5}NbO_4$ microwave dielectric ceramics based on structural refinement. Ceram Int. 2017;43(14):11516–22.
38. Brese NE, O'Keeffe M. Bond-valence parameters for solids. Acta Crystallogr B. 1991;47(2):192–7.
39. Kroumova E, Aroyo MI, Perez-Mato JM, Kirov A, Capillas C, Ivantchev S, et al. Bilbao crystallographic server: Useful databases and tools for phase-transition studies. Phase Transitions. 2003;76(1–2):155–70.
40. Lai YM, Tang XL, Zhang HW, Huang X, Li J, Su H. Relationship between the structure and microwave dielectric properties of non-stoichiometric $Li_{2+x}SiO_3$ ceramics. Ceram Int. 2017;43(2):2664–9.
41. Zhang X, Tang B, Fang ZX, Yang HY, Xiong Z, Xue LX, et al. Structural evolution and microwave dielectric properties of a novel $Li_3Mg_{2-x/3}Nb_{1-2x/3}Ti_xO_6$ system with a rock salt structure. Inorg Chem Front. 2018;5(12):3113–25.
42. Zhang Y, Zhang YC, Xiang MQ. Crystal structure and microwave dielectric characteristics of Zr-substituted $CoTiNb_2O_8$ ceramics. J Eur Ceram Soc. 2016;36(8):1945–51.
43. Breeze JD, Perkins JM, McComb DW, Alford NM. Do grain boundaries affect microwave dielectric loss in oxides? J Am Ceram Soc. 2009;92(3):671–4.
44. Ichinose N, Shimada T. Effect of grain size and secondary phase on microwave dielectric properties of $Ba(Mg_{1/3}Ta_{2/3})O_3$ and $Ba([Mg,Zn]_{1/3}Ta_{2/3})O_3$ systems. J Eur Ceram Soc. 2006;26(10):1755–9.
45. Song J, Zhang J, Zuo R. Ultrahigh Q values and atmosphere-controlled sintering of $Li_{2(1+x)}Mg_3ZrO_6$ microwave dielectric ceramics. Ceram Int. 2017;43(2):2246–51.
46. Shannon RD, Rossman GR. Dielectric constants of silicate garnets and the oxide additivity rule. Am Mineral. 1992;77(1–2):94–100.
47. Penn SJ, Alford NM, Templeton A, Wang X, Xu M, Reece M, et al. Effect of porosity and grain size on the microwave dielectric properties of sintered alumina. J Am Ceram Soc. 1997;80(7):1885–8.
48. Shannon RD. Dielectric polarizabilities of ions in oxides and fluorides. J Appl Phys. 1993;73(1):348–66.
49. Huang CL, Yang WR, Yu PC. High-Q microwave dielectrics in low-temperature sintered $(Zn_{1-x}Ni_x)_3Nb_2O_8$ ceramics. J Eur Ceram Soc. 2014;34(2):277–84.
50. Pan HL, Cheng L, Wu HT. Relationships between crystal structure and microwave dielectric properties of $Li_2(Mg_{1-x}Co_x)_3TiO_6$ ($0 \le x \le 0.4$) ceramics. Ceram Int. 2017;43(17):15018–26.

SUPPORTING INFORMATION

Additional supporting information may be found online in the Supporting Information section at the end of the article.

How to cite this article: Wang G, Zhang D, Huang X, et al. Crystal structure and enhanced microwave dielectric properties of Ta^{5+} substituted $Li_3Mg_2NbO_6$ ceramics. *J Am Ceram Soc*. 2019;00:1–10. https://doi.org/10.1111/jace.16692